

Effect of small amounts of hydrogen added to argon glow discharges: Hybrid Monte Carlo–fluid model

Annemie Bogaerts* and Renaat Gijbels

Department of Chemistry, University of Antwerp, Universiteitsplein 1, B-2610 Wilrijk-Antwerp, Belgium

(Received 3 October 2001; revised manuscript received 13 December 2001; published 26 April 2002)

A hybrid Monte Carlo–fluid modeling network is developed for an argon-hydrogen mixture, to predict the effect of small amounts of hydrogen added to a dc argon glow discharge. The species considered in the model include the Ar gas atoms, electrons, Ar^+ ions and fast Ar atoms, ArH^+ , H^+ , H_2^+ and H_3^+ ions, and H atoms and H_2 molecules, as well as Ar metastable atoms, sputtered Cu atoms, and the corresponding Cu^+ ions. Sixty-five reactions between these species are incorporated in the model. The effect of hydrogen on various calculation results is investigated, such as the species densities, the relative role of different production and loss processes for the various species, the cathode sputtering rate and contributions by different bombarding species, and the dissociation degree of H_2 and the ionization degree of Ar and Cu. The calculation results are presented and discussed for 1% H_2 addition, and comparison is also made with a pure argon discharge and with only 0.1% H_2 addition.

DOI: 10.1103/PhysRevE.65.056402

PACS number(s): 52.65.–y

I. INTRODUCTION

In recent years, there has been a lot of interest in the effects of small amounts of hydrogen added to argon discharges [1–18]. The addition of hydrogen was found to cause a drop in the ionization in the discharge, and in the Ar ion and electron densities [1–4]. It is also well-recognized that the addition of hydrogen affects the sputter rates in glow discharges [5,6]. On one hand, the sputter yield by hydrogen ions is very low, due to their low mass [5]. But on the other hand, the ArH^+ ions formed in argon-hydrogen discharges start playing an important role in sputtering, due to their higher kinetic energy than Ar^+ ions when bombarding the cathode [6]. A number of papers have also reported on the measurement of ion energy distributions in argon/hydrogen discharges [7–9]. The dissociation rate of H_2 in argon-hydrogen mixtures was also investigated, and it was found to be much smaller than in pure hydrogen discharges, as a result of vibration-translation energy exchanges [10]. Hydrogen Balmer lines were measured in argon-hydrogen glow discharges to obtain information on reactions in the plasma [11], on the electron density [12], and on the electric field distribution [13]. Moreover, the effect of hydrogen has also been investigated on glow discharges used for the spectrochemical analysis of solid materials by cathode sputtering. It has been observed that some optical emission line intensities of Ar atoms and ions, and of sputtered (e.g., copper) atoms and ions, increase while others decrease when hydrogen is added [14–16]. Also, the relative ionization efficiencies of different sputtered elements in these glow discharges appear to be influenced by the addition of hydrogen [17,18].

Although a large number of chemical reactions have been studied between argon and hydrogen species [19–31], the various effects of hydrogen on argon discharges are not fully understood. In order to obtain a better understanding of these

effects, we have developed a comprehensive modeling network, based on various Monte Carlo (MC) and fluid models, for the different species present in argon-hydrogen glow discharges. There exist some models in the literature for pure hydrogen discharges [32–39], but to our knowledge, there is only one model published for an argon-hydrogen mixture [40], which was simply based on particle balance equations, and applied to a thermal argon-hydrogen plasma, hence operating at completely different discharge conditions from a (nonthermal) glow discharge.

II. DESCRIPTION OF THE MODELING NETWORK

Thirteen different species are considered in the model, including the Ar gas atoms, electrons, Ar^+ , ArH^+ , H^+ , H_2^+ and H_3^+ ions, fast Ar atoms, H atoms, and H_2 molecules, the Ar metastable atoms, the sputtered cathode atoms (Cu is taken as an example) and the Cu^+ ions.

For the Ar gas atoms, no model is used, and they are simply assumed to be uniformly distributed in the plasma, with thermal velocities. Their density is calculated from the input gas pressure and temperature, by the ideal gas law ($n = N/V = p/kT$), multiplied by the percentage argon [i.e., 1 – (percentage hydrogen)]. The behavior of the other species is described by a number of MC models (for the species that are not in equilibrium with the electric field, i.e., they gain more energy from the electric field than they lose by collisions; hence, a MC model is most accurate) and fluid models (for the species that can be considered in equilibrium with the electric field; hence, a fluid model is a valid approach). In the following, these different models will be explained in some more detail, and the coupling between the different models, due to the interaction processes between the different species, will be outlined.

A. MC model for the electrons

The electrons are described by using a MC model during successive time steps, from the moment they are created (ei-

*Email address: annemie.bogaerts@ua.ac.be

TABLE I. Reactions taken into account in the electron MC model.

No.	Reaction	Name	Ref.
1	$e^- + \text{Ar} \rightarrow e^- + \text{Ar}$	Elastic scattering	[41]
2	$e^- + \text{Ar} \rightarrow e^- + \text{Ar}^+ + e^-$	Ionization	[41]
3	$e^- + \text{Ar} \rightarrow e^- + \text{Ar}^*$ (including Ar_m^*)	Total excit. (including the Ar metast. levels)	[41]
4	$e^- + \text{Ar}_m^* \rightarrow e^- + \text{Ar}^+ + e^-$	Ionization from the Ar metast. levels	[44]
5	$e^- + \text{Ar}_m^* \rightarrow e^- + \text{Ar}^*$	Total excitation from the Ar metast. levels	[45]
6	$e^- + \text{H}_2 \rightarrow e^- + \text{H}_2$	Elastic scattering	[46]
7	$e^- + \text{H}_2 \rightarrow e^- + \text{H}_2^*(v)$	Total vibrational excitation	[46]
8	$e^- + \text{H}_2 \rightarrow e^- + \text{H}_2^*(s)$	Total electron excitation to singlet states	[46]
9	$e^- + \text{H}_2 \rightarrow e^- + \text{H}_2^*(t) \rightarrow e^- + \text{H} + \text{H}$	Total electron excitation to triplet states, followed by dissociation	[46]
10	$e^- + \text{H}_2 \rightarrow e^- + \text{H}_2^+ + e^-$	Ionization	[46]
11	$e^- + \text{H}_2 \rightarrow e^- + \text{H}^+ + \text{H} + e^-$	Dissociative ionization	[47]
12	$e^- + \text{H} \rightarrow e^- + \text{H}^*$	Total excitation	[49]
13	$e^- + \text{H} \rightarrow e^- + \text{H}^+ + e^-$	Ionization	[49]
14	$e^- + \text{Cu} \rightarrow e^- + \text{Cu}^+ + e^-$	Ionization	[50]

ther by secondary electron emission at the cathode, or by ionization in the plasma), until they bombard the walls (where they can be reflected, cause secondary electron emission or become absorbed), or until they become thermalized in the negative glow (NG) (see below).

The secondary electron emission can be caused either by Ar^+ ions, fast Ar atoms, ArH^+ , H^+ , H_2^+ or H_3^+ ions bombarding the cathode. The emission yields for Ar^+ ion and Ar atom bombardment, as a function of the incoming energy (which is calculated in the MC models for ions and atoms; see below), are adopted from Ref. [41], whereas the corresponding values for H^+ , H_2^+ , and H_3^+ ions are taken from Ref. [42]. We could not find experimental data for ArH^+ -ion-induced emission yields. However, because of the large proton affinity for Ar, ArH^+ ions have probably not sufficient internal energy for potential ejection of secondary electrons. For kinetic ejection of secondary electrons, we can assume that the secondary electron emission yield is equal to that for an Ar atom (with energy equal to 40/41 of the ArH^+ energy) plus the contribution from an independently acting H^+ ion (with energy equal to 1/41 of the ArH^+ energy) [43].

The electrons emitted from the cathode are accelerated in the cathode dark space (CDS) by the strong electric field, and they are subject to collisions in the plasma. The collision processes taken into account in this model are summarized in Table I, together with the references of the corresponding cross sections [41,44–50]. The elastic scattering reactions (nos. 1 and 6) lead to a change in direction of the electrons but nearly no change in the energy, due to the large difference in mass of electrons and Ar atoms or H_2 molecules. The different electron impact ionization reactions (i.e., nos. 2, 4, 10, 11, 13, and 14) give rise to a new electron that is also followed in this electron MC model, and an ion that is treated in the ion MC models described below. Two kinds of electron impact excitation are considered in this model, i.e., total vibrational excitation of H_2 molecules (no. 7, which in our model leads only to a change in energy and direction of the electrons, because the vibrationally excited H_2 molecules

are not explicitly followed in the model) and total electronic excitation (nos. 3, 5, 8, 9, and 12). It should be mentioned that reaction no. 3 stands for total electronic excitation of Ar (i.e., summed over all Ar excited levels), but the excitation to the Ar metastable levels is also explicitly described in the model, because it is necessary as input for the Ar metastable model (see below). Similarly, electron impact ionization and excitation from the Ar metastable level (reactions nos. 4 and 5) are included in the MC model, because they are also used as input in the Ar metastable model.

Electronic excitation of the H_2 molecules can lead either to singlet or triplet states. In our model we use only two electronic excitation cross sections for H_2 , i.e., for the sum over all singlet states and for the sum over all triplet states. It is generally known that excitation to the triplet states leads to dissociation of the H_2 molecule. Indeed, all triplet states will radiate to the lowest triplet H_2 state ($b^3\Sigma_u^+$) [48], which is formed by two H ground state atoms, in which one electron is in a binding orbital and the other in an antibinding orbital. This state is repulsive, and will consequently dissociate into two H atoms. Moreover, we assume that also about 15% of the singlet excitation leads to dissociation, based on the cross sections of photon emission for the Ly- α , Ly- β , H- α , H- β , H- γ , H- δ lines and the production of metastable H($2s$) atoms, found in Ref. [47]. Therefore, the total dissociation rate of H_2 due to electron impact excitation is calculated in our model as the sum of the total triplet excitation rate + 15% of the total singlet excitation rate. Finally, rotational excitation of H_2 is neglected in the model, because (i) the energy loss is small, and it has no effect on the electron energy distribution function, and (ii) the rotationally excited H_2 molecules are not considered in the model.

As mentioned above, the electrons are followed in this MC model during successive time steps, until they bombard the walls, or until they become thermalized in the NG. In contrast to our previous electron MC model for pure argon discharges, where electrons with energy below 11.55 eV in the NG were transferred to the slow electron group (to be

treated in the fluid model) [51], all electrons with energy above thermal energy are followed in the present MC model. Indeed, because of the presence of H_2 molecules, the threshold for inelastic collisions is now reduced to about 0.5 eV (i.e., for vibrational excitation of H_2). In order to limit the calculation time when a large number of slow electrons has to be simulated, a variable time step (depending on the electron energy) is used to calculate the electron trajectories in the NG.

B. MC models for the Ar^+ , ArH^+ , H^+ , H_2^+ , and H_3^+ ions and the fast Ar atoms

The slow electrons are described with a fluid model in the NG, where they can be considered in equilibrium with the weak electric field. This fluid model describes also the various ionic species, as will be explained in Sec. II C. However, in addition to this fluid model, we have also developed a number of MC models in the CDS for the various ionic species (Ar^+ , ArH^+ , H^+ , H_2^+ , and H_3^+), as well as for the fast Ar atoms created from the ions by various kinds of collisions. Indeed, the ions are not in equilibrium with the strong electric field in the CDS, and are therefore more accurately treated with a MC code. Moreover, we are interested in the flux energy distributions of the ionic species and the fast Ar atoms bombarding the cathode (i.e., to calculate the secondary electron emission yields and the sputtering yields; see above and below, respectively), which can be easily calculated in the MC model.

The flux of the ions entering the CDS from the NG is obtained from the fluid model (see below). The ions are then accelerated toward the cathode by the strong electric field, and they are also subject to collisions. Table II gives an overview of the reactions taken into account in the MC models for Ar^+ , ArH^+ , H^+ , H_2^+ , and H_3^+ ions and fast Ar atoms, respectively, as well as the references where the cross sections were taken from [28,29,43,49,52–57].

Some reactions, such as elastic scattering (including symmetric charge transfer), do not result in the creation of new species; they only change the energy and direction of the ions and atoms. However, most other reactions, such as proton transfer, asymmetric charge transfer, collision-induced dissociation, etc., lead to the destruction of the ions, and the formation of new types of ions and/or neutrals. These created species are also followed in the MC models (for the ionic species and the fast Ar atoms), as well as in the fluid models (for the ions, the H atoms, and H_2 molecules; see below).

Reaction nos. 17 and 50; i.e., fast Ar^+ ion and Ar atom impact ionization, give rise to a new electron and an (additional) Ar^+ ion; the latter is also followed in the Ar^+ MC model, whereas the electron is followed in the electron MC model (see above). Finally, reaction nos. 18 and 51 are fast Ar^+ ion and Ar atom impact excitation to the Ar metastable level. The corresponding excitation rates are used as input in the Ar metastable model (see below).

All the ions that enter the CDS from the NG, as well as the ones created from collisions of the other species in the CDS (see Table II) are followed, until they are destroyed by collisions (see above) or until they bombard the cathode (or

the other cell walls), where they are assumed to be reflected as neutrals. The Ar^+ ions (as well as the Ar atoms) are assumed to be reflected for 100% as neutral Ar atoms, with a fraction of their initial kinetic energy; the latter is adopted from Ref. [58]. The H^+ , H_2^+ , H_3^+ , and ArH^+ ions are assumed to be reflected as H atoms, with a reflection probability of 0.6, 1.2, 1.8, and 0.6, respectively [59]. The H atoms are not followed by using a MC algorithm, but their production rate due to reflection is used as input in the H- H_2 fluid model (see below).

The fast Ar atoms, created (i) by neutralized reflection at the walls of the Ar^+ ions, (ii) by collisions of the various ions in the CDS (see Table II), or (iii) from other fast Ar atoms by elastic collisions in the plasma or reflection at the walls, are followed by using the MC method, until their energy drops below 1 eV, because at lower energy, they are not assumed to be “fast” anymore.

C. Fluid model for electrons, Ar^+ , ArH^+ , H^+ , H_2^+ , and H_3^+ ions

As mentioned above, the various ionic species and the slow electrons are also treated with a fluid model. It consists of six continuity (balance) equations and six transport equations (based on diffusion and migration), i.e., one for each type of species:

$$\frac{\partial n_x}{\partial t} + \vec{\nabla} \cdot \vec{J}_x = R_{\text{prod},x} - R_{\text{loss},x},$$

$$\vec{J}_x = \pm \mu_x n_x \vec{E} - D_x \vec{\nabla} n_x.$$

Here, x stands for every type of species (Ar^+ , ArH^+ , H^+ , H_2^+ , H_3^+ or electrons), n and j denote the species density and flux, R_{prod} and R_{loss} are the species total production and loss rates, μ and D are the species mobility and diffusion coefficients, and E is the electric field distribution. In the transport equation, a positive sign in the migration term is used for the ions, whereas a negative sign applies to the electrons. The mobility and diffusion coefficients for the Ar^+ ions and electrons were taken from Ref. [51]. The diffusion coefficients for the ArH^+ , H^+ , H_2^+ , and H_3^+ ions in argon/hydrogen are calculated with a formula of the rigid-sphere model for a mixture of two chemical species [60]. The mobilities of ArH^+ and H_3^+ ions in argon/hydrogen are adopted from Ref. [61], and due to the lack of available data, the same values were also assumed for H^+ and H_2^+ ions. The following production and loss processes were taken into account for the various species (the numbers between brackets correspond to the numbers given in Tables I and II, for the processes treated in the MC codes).

(a) *Production of electrons.* Electron (2), fast Ar ion (17), and atom (50) impact ionization of Ar, electron impact ionization of Ar metastable atoms (4), of sputtered Cu atoms (14), of H atoms (13) and of H_2 molecules (10), and dissociative ionization of H_2 (11).

(b) *Loss of electrons.* Recombination with ArH^+ , H_2^+ , and H_3^+ ions ($k = 10^{-7} \text{ cm}^3 \text{ s}^{-1}$ in the three cases [3,37,40]).

TABLE II. Reactions taken into account in the MC models for Ar^+ , ArH^+ , H^+ , H_2^+ , H_3^+ ions and fast Ar atoms.

No.	Reaction	Name	Ref.
Ar⁺ ions			
15	$\text{Ar}^+ + \text{Ar} \rightarrow \text{Ar}^+ + \text{fast Ar}$	Elastic (isotropic) scattering ^a	[52]
16	$\text{Ar}^+ + \text{Ar} \rightarrow \text{fast Ar} + \text{slow Ar}^+$	Elastic scattering in backward direction ^a	[52]
17	$\text{Ar}^+ + \text{Ar} \rightarrow \text{Ar}^+ + \text{Ar}^+ + e^-$	Ionization	[53]
18	$\text{Ar}^+ + \text{Ar} \rightarrow \text{Ar}^+ + \text{Ar}_m^*$	Excitation to the metastable levels	[53]
19	$\text{Ar}^+ + \text{H}_2 \rightarrow \text{ArH}^+ + \text{H}$	H-atom transfer	[54]
20	$\text{Ar}^+ + \text{H}_2 \rightarrow \text{fast Ar} + \text{H}_2^+$	Asymmetric charge transfer	[54]
ArH⁺ ions			
21	$\text{ArH}^+ + \text{Ar} \rightarrow \text{ArH}^+ + \text{fast Ar}$	Elastic scattering	[43]
22	$\text{ArH}^+ + \text{Ar} \rightarrow \text{fast Ar} + \text{H}^+ + \text{Ar}$	Collision-induced dissociation	[43]
23	$\text{ArH}^+ + \text{Ar} \rightarrow \text{fast Ar}^+ + \text{H} + \text{Ar}$	Collision-induced dissociation	[43]
24	$\text{ArH}^+ + \text{H}_2 \rightarrow \text{ArH}^+ + \text{fast H}_2$	Elastic scattering	[43]
25	$\text{ArH}^+ + \text{H}_2 \rightarrow \text{fast Ar} + \text{H}_3^+$	Proton transfer	[43]
H⁺ ions			
26	$\text{H}^+ + \text{Ar} \rightarrow \text{H}^+ + \text{fast Ar}$	Elastic scattering	[43,55]
27	$\text{H}^+ + \text{Ar} \rightarrow \text{fast H} + \text{Ar}^+$	Asymmetric charge transfer	[54]
28	$\text{H}^+ + \text{H} \rightarrow \text{fast H} + \text{H}^+$	Symmetric charge transfer	[49]
29	$\text{H}^+ + \text{H}_2 \rightarrow \text{H}^+ + \text{H}_2^*$	Total vibrational excitation	[56,57]
30	$\text{H}^+ + \text{H}_2 \rightarrow \text{H}^+ + \text{fast H}_2$	Elastic scattering	[56,57]
31	$\text{H}^+ + \text{H}_2 \rightarrow \text{fast H} + \text{H}_2^+$	Asymmetric charge transfer	[56,57]
H₂⁺ ions			
32	$\text{H}_2^+ + \text{Ar} \rightarrow \text{H} + \text{ArH}^+$	Proton transfer	[43,54]
33	$\text{H}_2^+ + \text{Ar} \rightarrow \text{fast H}_2 + \text{Ar}^+$	Asymmetric charge transfer	[43,54]
34	$\text{H}_2^+ + \text{H}_2 \rightarrow \text{H} + \text{H}_3^+$	Proton transfer	[56,57]
35	$\text{H}_2^+ + \text{H}_2 \rightarrow \text{fast H}_2 + \text{H}_2^+$	Symmetric charge transfer	[56,57]
H₃⁺ ions			
36	$\text{H}_3^+ + \text{Ar} \rightarrow \text{H}_3^+ + \text{fast Ar}$	Elastic scattering	[28,43,54]
37	$\text{H}_3^+ + \text{Ar} \rightarrow \text{fast H}_2 + \text{slow ArH}^+$	Proton transfer	[28,43,54]
38	$\text{H}_3^+ + \text{Ar} \rightarrow \text{fast H}_2 + \text{fast H} + \text{slow Ar}^+$	Charge transfer+ dissociation	[28,43,54]
39	$\text{H}_3^+ + \text{Ar} \rightarrow \text{fast H}^+ + \text{fast H}_2 + \text{slow Ar}$	Collision-induced dissociation	[28,43,54]
40	$\text{H}_3^+ + \text{Ar} \rightarrow \text{fast H}_2^+ + \text{fast H} + \text{slow Ar}$	Collision-induced dissociation	[28,43,54]
41	$\text{H}_3^+ + \text{H}_2 \rightarrow \text{H}_3^+ + \text{fast H}_2$	Elastic scattering	[29,43,56]
42	$\text{H}_3^+ + \text{H}_2 \rightarrow \text{fast H}_2 + \text{slow H}_3^+$	Proton transfer	[29,43,56]
43	$\text{H}_3^+ + \text{H}_2 \rightarrow \text{fast H}_2 + \text{slow H}_2 + \text{slow H}^+$	Proton transfer+ dissociation	[29,43,56]
44	$\text{H}_3^+ + \text{H}_2 \rightarrow \text{fast H}_2 + \text{slow H} + \text{slow H}_2^+$	Proton transfer+ dissociation	[29,43,56]
45	$\text{H}_3^+ + \text{H}_2 \rightarrow \text{fast H}_2 + \text{fast H} + \text{slow H}_2^+$	Charge transfer+ dissociation	[29,43,56]
46	$\text{H}_3^+ + \text{H}_2 \rightarrow \text{fast H}_2^+ + \text{fast H} + \text{slow H}_2$	Collision-induced dissociation	[29,43,56]
47	$\text{H}_3^+ + \text{H}_2 \rightarrow \text{fast H}^+ + \text{fast H}_2 + \text{slow H}_2$	Collision-induced dissociation	[29,43,56]
48	$\text{H}_3^+ + \text{H}_2 \rightarrow \text{fast H}^+ + \text{two fast H} + \text{slow H}_2$	Collision-induced dissociation	[29,43,56]
Fast Ar atoms			
49	$\text{fast Ar} + \text{slow Ar} \rightarrow \text{fast Ar} + \text{fast Ar}$	Elastic scattering	[52]
50	$\text{fast Ar} + \text{slow Ar} \rightarrow \text{fast Ar} + \text{Ar}^+ + e^-$	Ionization	[53]
51	$\text{fast Ar} + \text{slow Ar} \rightarrow \text{fast Ar} + \text{Ar}_m^*$	Excitation to the metastable levels	[53]

^aWe have represented the differential cross section for elastic scattering of Ar^+ ions by Ar atoms by the sum of an isotropic term and a backward scattering term. The integral over angles of the backward scattering term is equal to the symmetric charge transfer cross section at energies above about 1 eV.

(c) *Production of Ar⁺*. Electron (2), fast Ar ion (17) and atom (50) impact ionization of Ar, electron impact ionization of Ar metastable atoms (4), collision-induced dissociation of ArH⁺ ions with Ar (23), charge transfer of H⁺ (27), H₂⁺ (33), and H₃⁺ (38) ions with Ar atoms.

(d) *Loss of Ar⁺*. H atom transfer (19) and charge transfer (20) of Ar⁺ ions with H₂ molecules.

(e) *Production of ArH⁺*. H-atom transfer of Ar⁺ with H₂ (19), proton transfer of H₂⁺ (32) and of H₃⁺ (37) with Ar.

(f) *Loss of ArH⁺*. Electron-ion recombination, collision-induced dissociation with Ar (22, 23), proton transfer with H₂ (25).

(g) *Production of H⁺*. Electron impact ionization of H (13) and dissociative ionization of H₂ (11), collision-induced dissociation of ArH⁺ with Ar (22), collision-induced dissociation of H₃⁺ with Ar (39) and with H₂ (47, 48), proton transfer plus dissociation of H₃⁺ with H₂ (43).

(h) *Loss of H⁺*. Charge transfer with Ar (27) and with H₂ (31).

(i) *Production of H₂⁺*. Electron impact ionization of H₂ (10), charge transfer of Ar⁺ (20) and of H⁺ (31) with H₂, collision-induced dissociation of H₃⁺ with Ar (40) and with H₂ (46), proton transfer plus dissociation (44) and charge transfer plus dissociation (45) of H₃⁺ with H₂.

(j) *Loss of H₂⁺*. Electron-ion recombination, proton transfer (32) and charge transfer (33) of H₂⁺ with Ar, and proton transfer with H₂ (34).

(k) *Production of H₃⁺*. Proton transfer of ArH⁺ (25) and of H₂⁺ (34) with H₂.

(l) *Loss of H₃⁺*. Electron-ion recombination, proton transfer (37), charge transfer plus dissociation (38) and collision-induced dissociation (39,40) with Ar, proton transfer plus dissociation (43,44), charge transfer plus dissociation (45) and collision-induced dissociation (46,47,48) with H₂.

Most of the production and loss rates are calculated in the MC models, i.e., in the entire discharge for the electron-induced reactions, and in the CDS for the ion-induced processes. However, in addition, some of the ion-induced chemical reactions are also treated in the fluid model itself, i.e., when the cross section is high at thermal energy, so that the process can occur with thermal ions in the NG. This is the case for reactions 19, 20, 25, 32, 33, and 34 (see references for the cross sections). The additional production and loss rates are then calculated based on the densities of the collision partners multiplied with the rate coefficients, which are calculated from the cross sections at thermal energy. The values calculated in this way appear to be in good agreement with rate coefficients found in the literature [30,40,62,63]. Finally, electron-ion recombination, which was not considered in the MC models because it applies to thermal electrons, is also treated in the fluid model. Only recombination with the molecular ions (ArH⁺, H₂⁺, and H₃⁺) is taken into account, and the rate coefficients used [3,37,40] are also given above between brackets. Recombination with atomic ions (Ar⁺ and H⁺) is negligible because of too low rate coefficients.

Finally, the above continuity and transport equations are coupled to Poisson's equation, to calculate the electric field distribution from the different ion and the electron densities:

$$\vec{\nabla} \cdot \vec{E} = \frac{e}{\epsilon_0} (n_{\text{Ar}^+} + n_{\text{ArH}^+} + n_{\text{H}^+} + n_{\text{H}_2^+} + n_{\text{H}_3^+} - n_e).$$

The set of coupled differential equations is solved with the Scharfetter-Gummel exponential scheme [51,64].

D. Fluid model for the H atoms and H₂ molecules

The H atoms and H₂ molecules are also described with a set of two coupled continuity (balance) equations (with different production and loss terms) and two transport equations (determined by diffusion),

$$\frac{\partial n_x}{\partial t} + \vec{\nabla} \cdot \vec{J}_x = R_{\text{prod},x} - R_{\text{loss},x},$$

$$\vec{J}_x = -D_x \vec{\nabla} n_x.$$

The production and loss processes taken into account are listed below.

(1) *Production of H*. Electron impact dissociative excitation (9) and ionization (11) of H₂, H-atom transfer of Ar⁺ with H₂ (19), collision-induced dissociation of ArH⁺ with Ar (23), charge transfer of H⁺ with Ar (27) and with H₂ (31), proton transfer of H₂⁺ with Ar (32) and with H₂ (34), charge transfer plus dissociation (38) and collision-induced dissociation (40) of H₃⁺ with Ar, proton transfer plus dissociation (44), charge transfer plus dissociation (45) and collision-induced dissociation (46, 48) of H₃⁺ with H₂, electron recombination with ArH⁺, H₂⁺, and H₃⁺, dissociation of H₂ by Ar metastables, and reflection of ArH⁺, H⁺, H₂⁺ and H₃⁺ at the walls.

(2) *Loss of H*. Electron impact ionization of H (13) and recombination at the walls (H+H→H₂; γ=0.1).

(3) *Production of H₂*. Charge transfer of H₂⁺ with Ar (33), proton transfer (37), charge transfer plus dissociation (38) and collision-induced dissociation (39) of H₃⁺ with Ar, proton transfer plus dissociation (43) and collision-induced dissociation (47) of H₃⁺ with H₂, electron-H₃⁺ recombination, and recombination of two H atoms at the walls.

(4) *Loss of H₂*. Electron impact dissociative excitation (9), ionization (10) and dissociative ionization (11), of H₂, H-atom transfer (19) and charge transfer (20) of Ar⁺ with H₂, proton transfer of ArH⁺ with H₂ (25), charge transfer of H⁺ with H₂ (31), proton transfer of H₂⁺ with H₂ (34), and dissociation of H₂ by Ar metastables.

The numbers between brackets correspond again to the numbers given in Tables I and II. Again, most production and loss rates are calculated by using the MC models of ions and electrons. In addition, the ion-induced reactions with high cross sections at thermal energy (so that the reactions can occur in the NG, with thermal ions) are also treated in the

H-H₂-fluid model, based on the rate coefficients and the densities of the reacting species, in analogy to the above electron-ion fluid model.

Dissociation of H₂ by Ar metastables is also taken into account in this model, because this process has been demonstrated to be important in argon-hydrogen glow discharges, by the strong continuum emission in the spectral range of 220–440 nm [14–16,27]. The rate of this reaction is obtained based on the Ar metastable density calculated in the metastable model (see below) and the H₂ density, multiplied by the corresponding reaction rate coefficient (assumed to be $7 \times 10^{11} \text{ cm}^3 \text{ s}^{-1}$, based on values reported in Refs. [30], [65–67]).

Besides the chemical reactions taking place in the plasma, two processes occurring at the walls might play an important role in determining the H and H₂ densities, i.e., reflection at the walls of ArH⁺, H⁺, H₂⁺, and H₃⁺ ions under the form of H atoms (treated in the ion MC models; see above) and recombination of H atoms into H₂ molecules at the walls (which are assumed to be saturated with H atoms). The latter reaction, which defines a loss of the H atoms and a formation of H₂ molecules, is treated as the boundary condition in the balance equations of H atoms and H₂ molecules, using a recombination coefficient of 0.1 [35,68,69]. This wall recombination of H atoms is suggested to be the dominant production mechanism of H₂ molecules in argon-hydrogen supersonically expanding cascaded arc plasmas (where no H₂ molecules, but only Ar⁺, Ar, H⁺, H, and electrons, are assumed to leave the arc) [3].

E. Fluid model for the Ar metastable atoms

Because of the possibly important role of the Ar metastables in dissociation of the H₂ molecules (see above), the models developed for the hydrogen species should also be coupled with a model for the Ar metastable atoms. The metastable model used for this purpose has been developed previously [70], except that two extra processes, related to H₂, are now added to the model.

The behavior of the Ar metastable atoms is again described by a balance (continuity) equation containing different production and loss terms, and a transport equation determined by diffusion,

$$\frac{\partial n_{\text{Ar}_m^*}}{\partial t} + \vec{\nabla} \cdot \vec{J}_{\text{Ar}_m^*} = R_{\text{prod Ar}_m^*} - R_{\text{loss Ar}_m^*},$$

$$\vec{J}_{\text{Ar}_m^*} = -D_{\text{Ar}_m^*} \vec{\nabla} n_{\text{Ar}_m^*}.$$

The diffusion coefficient (D) is assumed to be $54 \text{ cm}^2 \text{ s}^{-1}$ at 1 Torr [70]. The production processes taken into account in the model are electron, Ar⁺ ion, and fast Ar atom impact excitation to the metastable level (for which the rates are calculated in the MC models; see above), as well as Ar⁺ ion–electron radiative recombination (which is actually found to be negligible, due to the small rate coefficient [70]). The loss processes include electron impact ionization and total excitation from the metastable level (also treated in the

electron MC model above), electron quenching (i.e., transfer to the nearby $4s$ resonant levels by low-energy electrons), collisions between two metastable atoms (resulting in ionization of one of the atoms, whereas the other is deexcited to the ground state; hence, this process results in the simultaneous loss of two metastable atoms), Penning ionization of the sputtered Cu atoms, and two-body and three-body collisions with Ar ground state atoms. More details about these processes and the rate coefficients used can be found in Ref. [70].

The additional loss processes, related to the hydrogen species, which are now added to the model, are excitation followed by dissociation of the H₂ molecules due to Ar metastable atoms (see above), and excitation of H atoms by Ar metastable atoms, both leading to deexcitation of the metastable level. The rate coefficients for these processes are taken as 7×10^{-11} and $4 \times 10^{-11} \text{ cm}^3 \text{ s}^{-1}$, respectively [30].

Finally, it should be mentioned that there is another loss mechanism for the Ar metastable atoms, given by diffusion toward the walls, and subsequent deexcitation at the walls. The boundary condition for this model is therefore defined as the metastable density being equal to zero at the cell walls [70].

F. Models for the sputtered Cu atoms and corresponding Cu⁺ ions

Because it has been reported in the literature that the addition of hydrogen to an argon glow discharge affects the sputtering [5,6], as well as the optical emission line intensities [14–16] and ionization efficiencies [7,8] of sputtered atoms, the present modeling network for an argon-hydrogen glow discharge also includes some models for the sputtered species, which were previously developed [71,72], and which will be briefly outlined here, taking Cu as an example.

The sputtering rate for the Cu cathode is calculated based on an empirical formula for the sputtering yield as a function of energy of the bombarding species [73], multiplied by the flux energy distributions of the various ions and the fast Ar atoms bombarding the cathode. The Cu atoms sputtered from the cathode have typical energies in the order of 5–10 eV, which they lose almost immediately by collisions with the Ar gas atoms, until they are thermalized. This thermalization process is described by a MC model [71].

The further behavior of the thermalized Cu atoms, i.e., their transport by diffusion, and the ionization of the Cu atoms, as well as the behavior of the Cu⁺ ions, is described by a fluid model, consisting of two coupled continuity equations and two transport equations (based on diffusion for the Cu atoms and on diffusion plus migration for the Cu⁺ ions). The production of Cu atoms is given by the product of the sputtering rate and the thermalization profile, whereas the loss of Cu atoms, which is equal to the production of Cu⁺ ions, is dictated by electron impact ionization, Penning ionization by Ar metastable atoms, and asymmetric charge transfer with Ar⁺ ions. No loss of Cu⁺ ions in the plasma is explicitly taken into account, but the boundary condition of the continuity equation accounts for their loss by recombination at the cell walls. More information about this Cu-Cu⁺

model can be found in Ref. [72].

Finally, a MC model is also developed for the Cu^+ ions in the CDS, because they are not in equilibrium with the strong electric field in this region, and because this MC model allows us to compute the Cu^+ ion flux energy distribution, needed to calculate the sputtering rate. More information about this MC model is given in Ref. [72].

G. Coupling between the different models in the entire modeling network

Because the different plasma species interact with each other, the models used to describe their behavior are coupled to each other, and are solved iteratively (i.e., the output of one model is used as input in the next model) until final convergence is reached. It is important to realize that different kinds of models (MC and fluid) are sometimes applied to the same species and/or in the same spatial regions, because they yield complementary information. Indeed, a MC model is used for the fast (i.e., nonthermal) electrons in the entire discharge, and a fluid model is applied to the various ions and the thermal electrons in the entire discharge. Transfer of data between the two models is the slow electron transfer rate (from the MC model to the fluid model), beside other production and loss rates for the ionic species (see below). Beside the fluid model for the ions, a MC model is also developed for the various ions (as well as for the fast Ar atoms), but only in the CDS, because it gives a more accurate description when the species are not in equilibrium with the electric field, and because it yields the energy distribution of the ions, necessary to calculate secondary electron emission yields and sputter rates. Transfer of data from the fluid model to the MC model is the flux of ions entering the CDS from the NG. Hence, both a MC and a fluid model are used for the ionic species in the CDS, but we have checked that both models yielded the same results with respect to densities and fluxes. Similarly, for the Cu ions, a fluid model is used in the entire discharge, and a MC model is applied in the CDS. The flux entering the CDS from the NG is again calculated in the fluid model, and used as input in the MC model.

The general input for the modeling network is the cell geometry, the gas pressure and temperature, and the discharge voltage, as well as transport coefficients and the cross sections and rate coefficients of the various processes described in the model. Because the present paper intends to show the capabilities of the modeling network by presenting results generally applicable to argon-hydrogen glow discharges, we consider as an example a simple cylindrically symmetrical cell geometry, with length and diameter equal to 1 cm. This permits the fluid calculations to be performed in two dimensions: axial and radial directions. The MC simulations are, however, carried out in three dimensions, because this is mathematically simpler and it reflects reality. The operating conditions taken as example are a dc voltage of 800 V, a gas pressure of 1 Torr, and a temperature of 300 K.

The simulations start with a run of the *electron-ion fluid model*, using arbitrary production and loss rates for the different species. This model gives us the electric field distribu-

tion throughout the plasma, and the fluxes and density profiles of the various ions and electrons. The latter are used as input in the *H-H₂-fluid model*, which uses, for the first iteration, also arbitrary production and loss rates for the reactions treated in the MC models. The results of this *H-H₂-fluid model* are, among others, the density profiles of the H atoms and H₂ molecules. Using the latter density profiles, as well as arbitrary rates for the production and loss processes treated in the MC models, a run of the *Ar metastable model* is carried out, yielding, among others, the Ar metastable atom density. The latter is inserted in the *H-H₂-fluid model* that gives updated results for the H and H₂ density profiles. A second iteration between the Ar metastable model and the *H-H₂-fluid model* is not necessary here, because the results of both models would not change by more than 1% (i.e., convergence is reached). Also, the coupling back of the *H-H₂-fluid model* to the *electron-ion-fluid model* is not carried out at this moment, because (i) the new H and H₂ densities do not significantly affect the calculation results of the *electron-ion-fluid model*, and (ii) a new (and unnecessary) run of the *electron-ion-fluid model* increases the overall computation effort of the modeling network.

The electric field distribution, as well as the fluxes of the various ions entering the CDS from the NG, both calculated in the *electron-ion-fluid model*, are used as input in the MC models. Moreover, the density profiles of the H atoms and H₂ molecules, and of the Ar metastable atoms, calculated with the *H-H₂-fluid model* and with the Ar metastable model, respectively, are inserted in the MC models. The *different MC models*, i.e., for the Ar^+ , ArH^+ , H^+ , H_2^+ , and H_3^+ ions, the fast Ar atoms and the electrons, are run consecutively. The output of one MC model (e.g., the creation rate of other species by chemical reactions in the plasma, or the secondary electron emission rate) is used as input in the other MC models. This consecutive running has to be repeated a few times, with updated output/input for the other models, until convergence is reached. This is defined here when the ion and Ar atom fluxes arriving at the cathode, stay constant within 1% (the remaining differences are due to statistics). Typically, about 10–15 consecutive runs have to be carried out before convergence is reached.

When convergence is reached within the MC models, the *electron-ion-fluid model*, the *H-H₂-fluid model*, and the Ar metastable model are calculated again, using now the appropriate production and loss rates, as obtained from the MC models. Indeed, the rates of electron-, ion-, and atom-induced reactions are calculated in the MC models for electrons, ions, and Ar atoms, respectively, as the number of collision events per unit volume and unit time ($\text{cm}^{-3} \text{s}^{-1}$). These rates are then used in the right-hand side of the balance equations of the species described in the fluid models. Running the fluid models then yields a new electric field distribution, new ion fluxes entering the CDS from the NG, and new density profiles of the plasma species. These new data are then again inserted in the MC models, and the procedure of consecutively running the MC models is repeated, in the same way as above. The iteration between the fluid models on one hand, and the various MC models on the other hand, has to be repeated until final convergence is

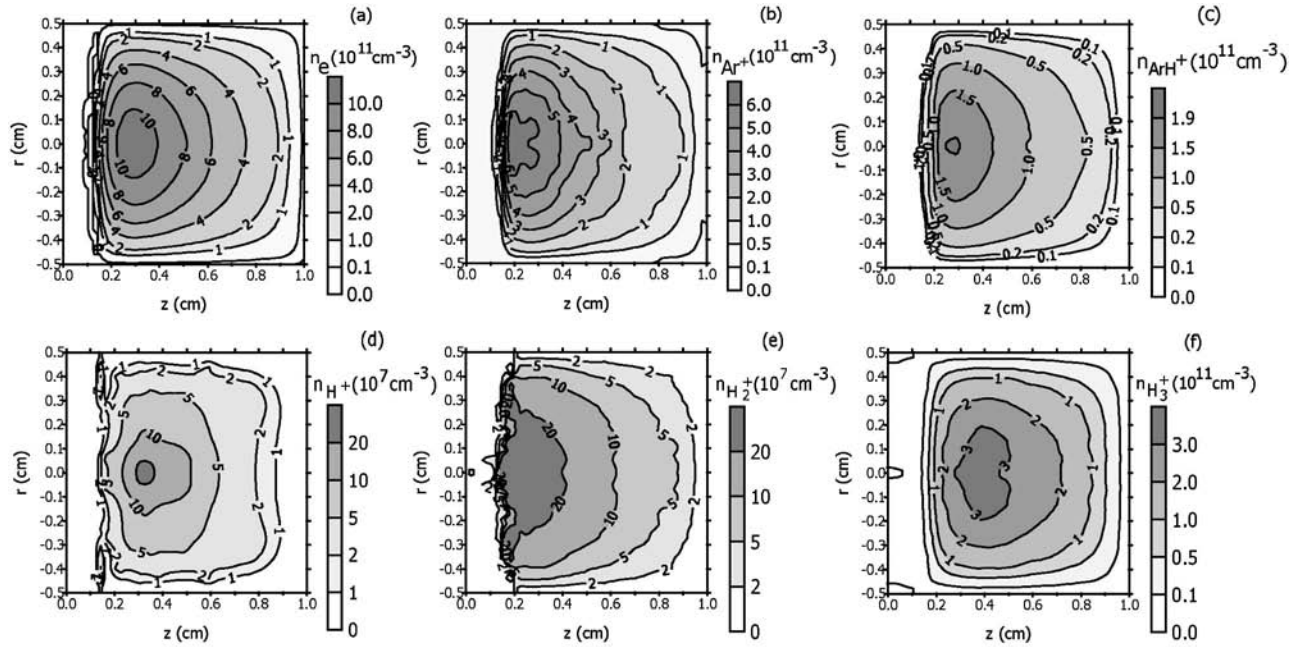


FIG. 1. Calculated two-dimensional density profiles of the electrons (a), Ar^+ ions (b), ArH^+ ions (c), H^+ ions (d), H_2^+ ions (e), and H_3^+ ions (f), in an Ar glow discharge with 1% H_2 addition at 800 V, 1 Torr, and 300 K. The cathode is found at the left end of the figure, whereas the other borders of the figure are at anode potential.

reached, which is defined when the ion fluxes bombarding the cathode as well as the electron and ion densities, all calculated in the electron-ion–fluid model, stay constant within 1%. This takes typically about 5–10 iterations, depending on the initial guesses for the production and loss rates. The whole calculation procedure can, therefore, amount to several days on a professional workstation with alpha-processor.

Once convergence is reached for the above-described models, *the models for the sputtered species* are calculated. The flux energy distributions of the various ions and the fast Ar atoms are used to calculate the amount of sputtering, and the thermalization profile of the sputtered Cu atoms. This is used as input in the Cu/Cu^+ –fluid model to calculate the further behavior of the Cu atoms and Cu^+ ions. Output of the latter model is, among others, the flux of Cu^+ ions entering the CDS from the NG, which is used in the Cu^+ MC model to calculate the trajectory of Cu^+ ions on their way toward the cathode. This yields, among others, the flux energy distribution of Cu^+ ions bombarding the cathode, which is used to calculate the updated sputtering rate. Hence, the MC model for thermalization of Cu atoms, the Cu/Cu^+ –fluid model, and the MC model for Cu^+ ions in the CDS are repeated until convergence is reached (determined when the sputtering rate does not change anymore). This happens already after 3 or 4 iterations.

Subsequently, the output of the three Cu models is inserted into the MC and fluid models for the electrons, argon, and hydrogen species. In practice, this has to be done only once, because the sputtered species appear to have only a minor effect on the other models. The main effect is on the Ar metastable atom density, through Penning ionization of the sputtered Cu atoms. The Ar metastable density changes,

however, typically by only a few percentages, and it has a negligible effect on the other models.

III. RESULTS AND DISCUSSION

To illustrate the results of the modeling network, it is applied to a simple cylindrically symmetrical glow discharge cell with length and diameter of 1 cm. Calculations have been performed for a dc discharge voltage of 800 V, a gas pressure of 1 Torr, and a gas temperature of 300 K. The corresponding electrical current is then calculated to be in the order of 5 mA (see below). These operating conditions have been taken as an example, because they are typical of sputtering glow discharges used for the spectrochemical analysis of solid materials; but the model can easily be applied to other dc glow discharge conditions as well.

Figure 1 shows the calculated two-dimensional density profiles of the electrons (a), Ar^+ ions (b), ArH^+ ions (c), H^+ ions (d), H_2^+ ions (e), and H_3^+ ions (f), in a mixture of Ar with 1% H_2 . The cathode is found at the left end of the figures (at $z=0$ cm), whereas the other borders of the figures are at anode potential. The density profiles of these species reach a maximum at about 2–3 mm from the cathode, which is in the beginning of the NG. The electron density is more or less zero in the CDS (which is about 1.5 mm thick at the conditions under study), whereas the various ion densities are characterized by low and rather constant (but nonzero) values in this region, giving rise to a positive space charge in the CDS. The NG, on the other hand, is characterized by nearly equal positive and negative space charges (i.e., charge neutrality).

The electron density [Fig. 1(a)] has a maximum somewhat above 10^{12} cm^{-3} , whereas the maximum Ar^+ ion den-

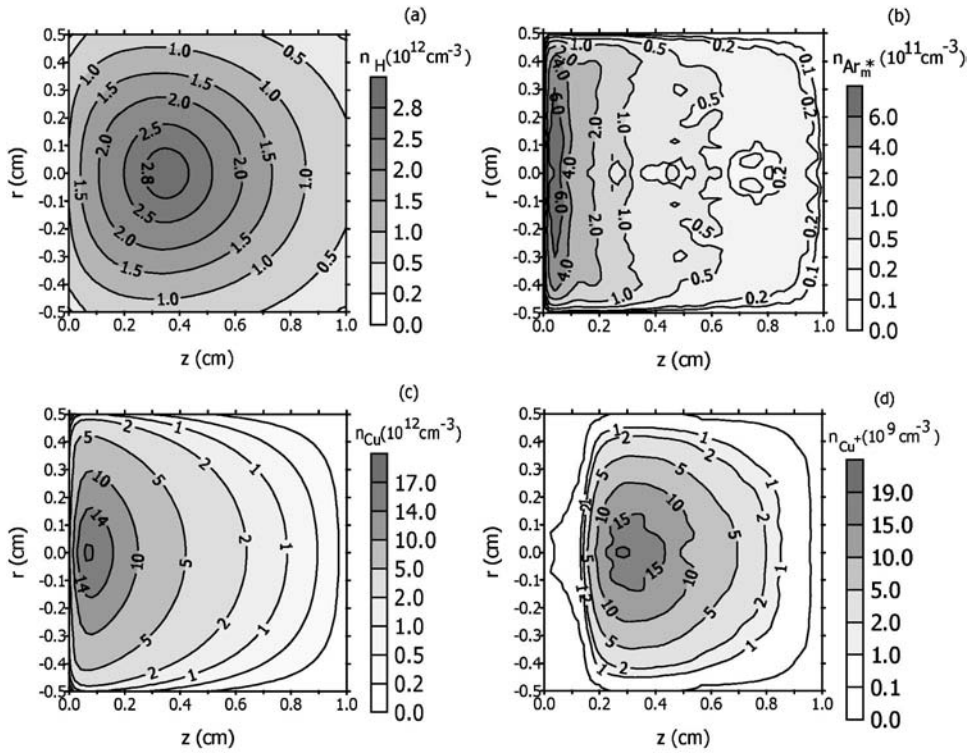


FIG. 2. Calculated two-dimensional density profiles of the H atoms (a), Ar metastable atoms (b), sputtered Cu atoms (c) and Cu^+ ions (d), in an Ar glow discharge with 1% H_2 addition at 800 V, 1 Torr, and 300 K.

sity [Fig. 1(b)] is about $6 \times 10^{11} \text{ cm}^{-3}$. Because the total ion density should be equal to the electron density in the NG, this means that the Ar^+ ions are the dominant ionic species in the plasma, at the conditions under study. However, the ArH^+ and H_3^+ ions have also rather high densities, with a maximum of about 2×10^{11} and $3 \times 10^{11} \text{ cm}^{-3}$, respectively [see Figs. 1(c) and 1(f)]. The densities of the H^+ and H_2^+ ions, on the other hand, are found to be negligible at the conditions under study [i.e., with maximum densities in the order of $2 \times 10^8 \text{ cm}^{-3}$; see Figs. 1(d) and 1(e)]. These results are, at least qualitatively, consistent with findings in the literature. Indeed, it is reported in Refs. [37,38] for pure hydrogen discharges that H^+ and H_2^+ ions react rapidly in low-field regions with H_2 molecules to form H_3^+ ions, which do not fragment again, until they move into higher field regions. H_3^+ ions are, therefore, the dominant hydrogen ions in low-field hydrogen plasmas [37,38,74–76]. Moreover, in glow discharge mass spectrometry the ArH^+ ion intensities in the mass spectrum are often found to be of the same magnitude or even higher than the Ar^+ ion intensity, when small amounts of H_2 (or H_2O) are added to the Ar glow discharge [17,77]. It is worth mentioning here that the ratios in the calculated ion densities illustrated in Fig. 1 are also reflected back in the ratios of the fluxes of the different ionic species.

The calculated two-dimensional density profiles of the other species present in the plasma, i.e., the H atoms, Ar metastable atoms, and sputtered Cu atoms and corresponding Cu^+ ions, are illustrated in Fig. 2. The density profiles of Ar gas atoms and H_2 molecules are not shown, because they are constant throughout the discharge. The total gas density at 1 Torr and 300 K is simply assumed constant and is calculated, based on the ideal gas law, to be equal to $3.22 \times 10^{16} \text{ cm}^{-3}$. At a mixture of 99% Ar with 1% H_2 , the Ar

gas atom density is then $3.19 \times 10^{16} \text{ cm}^{-3}$. The density of the H_2 molecules was calculated in the H- H_2 -fluid model, and was also found to be roughly uniform throughout the discharge, with a value of $3.22 \times 10^{14} \text{ cm}^{-3}$, i.e., exactly 1% of the total gas density, which was given as input (initial condition) in the model. Hence, this shows that the large number of production and loss processes taken into account in this model (see Sec. II) do not really affect the H_2 density at the conditions under study.

The H atom density, as calculated in the H- H_2 fluid model, was found to reach a maximum of almost $3 \times 10^{12} \text{ cm}^{-3}$ at about 3 mm from the cathode, and it decreases gradually toward the cell walls [see Fig. 2(a)]. This corresponds to a calculated dissociation degree of H_2 , integrated over the entire discharge region, of about 0.35%. Hence, this suggests that most of the added hydrogen is present in molecular form. On the other hand, although this value of 0.35% appears to be low, it should be mentioned that it is still several orders of magnitude higher than the ionization degree of Ar at the conditions under study (typically $10^{-5} - 10^{-6}$) [78]. Moreover, in spite of this low dissociation degree, the H atoms still have a quite high density (even higher than the electrons or any of the ionic species); hence they can be considered as one of the most abundant plasma species.

The Ar metastable atoms [Fig. 2(b)] appear to reach a pronounced maximum of $6 \times 10^{11} \text{ cm}^{-3}$ adjacent to the cathode, but the overall Ar metastable density in the plasma is calculated in the order of $2 \times 10^{10} - 2 \times 10^{11} \text{ cm}^{-3}$. The reason for this pronounced peak is the production of Ar metastable atoms by fast Ar ion and atom impact excitation, which is only important close to the cathode, where the Ar ions and atoms reach high enough energies for excitation [70].

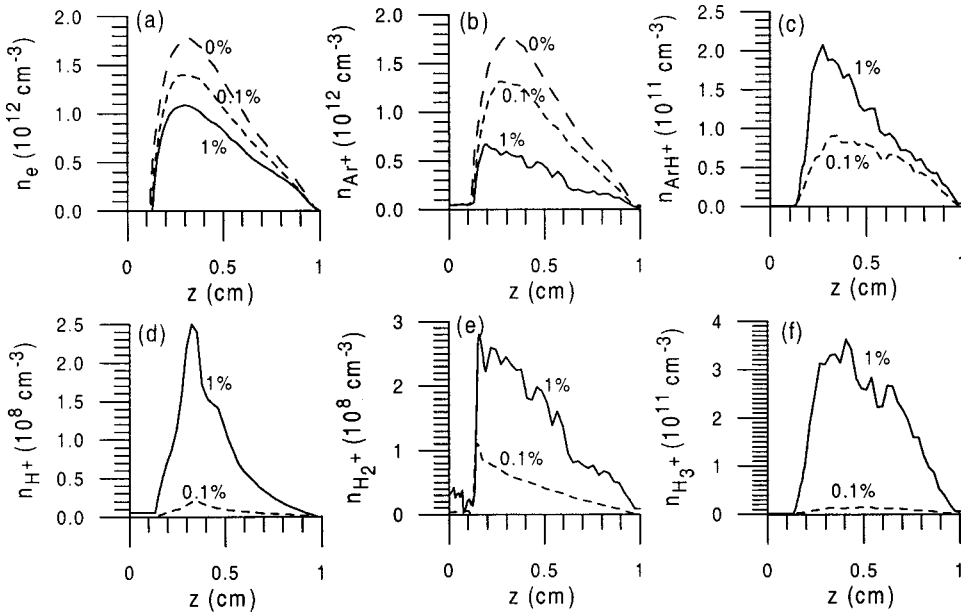


FIG. 3. Calculated one-dimensional density profiles (at the cell axis) of the electrons (a), Ar^+ ions (b), ArH^+ ions (c), H^+ ions (d), H_2^+ ions (e), and H_3^+ ions (f), in an Ar glow discharge with 1% H_2 addition (solid lines) and 0.1% H_2 addition (small dashed lines), and in a pure Ar discharge (wide dashed lines) at 800 V, 1 Torr, and 300 K.

The calculated Cu atom density [Fig. 2(c)] reaches also a maximum rather close to the cathode, which is logical because the Cu atoms are produced at the cathode due to sputtering. The reason that the maximum is not found back at the cathode surface itself is because the sputtered Cu atoms have initial energies in the order of a few eV, and they travel a certain distance before they are thermalized and start to move by diffusion [72,78]. Looking at the absolute values (i.e., a maximum of almost $2 \times 10^{13} \text{ cm}^{-3}$) tells us that the sputtered Cu atoms are quite abundant in the plasma, with a density of almost 0.1% of the argon gas atom density, and only one order of magnitude lower than the H_2 density, at the conditions under study (1% H_2 addition).

The corresponding Cu^+ ion density is calculated to be about three orders of magnitude lower, with a maximum of $2 \times 10^{10} \text{ cm}^{-3}$, at 2–3 mm from the cathode, hence at the same position as the electron and other ionic species densities (see Fig. 1). The ionization degree of Cu is hence calculated to be about 0.16%, which is somewhat lower than the dissociation degree of H_2 , but significantly higher than the calculated ionization degree of Ar (i.e., order of 10^{-5} ; see above and Ref. [78]). The reason is that the Cu atoms are not only ionized by electron impact ionization (which is the dominant ionization mechanism for the Ar atoms), but two other ionization processes, which are absent for argon, come into play, and are even more important, i.e., Penning ionization by Ar metastable atoms and asymmetric charge transfer with Ar^+ ions (see Sec. II F and also the paragraphs below).

In order to understand better the effect of hydrogen on an argon glow discharge, we have compared our calculation results for 1% H_2 addition with the results obtained for a pure Ar discharge. Figure 3 presents the one-dimensional density profiles (i.e., at the cell axis) of the electrons (a), Ar^+ (b), ArH^+ (c), H^+ (d), H_2^+ (e) and H_3^+ ions (f), for 1% H_2 addition (solid lines), in comparison with the pure Ar discharge (dashed line). Because the hydrogen-species are not present in the pure argon discharge, we have also carried out calculations for a lower H_2 fraction (i.e., 0.1%), to investigate the

effect of H_2 concentration on the hydrogen-related ions, and these results are illustrated with small dashed lines (also for the electrons and Ar^+ ions).

The electron and Ar^+ ion densities [Figs. 3(a) and 3(b)] drop with increasing H_2 addition. The effect is quite pronounced, even at the small H_2 concentration of 0.1%. The reason for this drop can be explained from the reactions taken into account in the model (see Sec. II).

The electrons are mainly created by electron impact ionization of Ar atoms (order of 90%), although fast Ar^+ ion and Ar atom impact ionization also play a non-negligible role (with contributions of several percentage). This is true both in the pure Ar discharge and in the Ar- H_2 mixture. Indeed, at the H_2 concentrations under study, electron impact ionization of H_2 molecules was found to be not so important because of the lower H_2 density (several orders of magnitude lower), and electron impact dissociative ionization of H_2 and ionization of H atoms, were found to be even less important. Hence, no additional production mechanisms of electrons play a significant role in the Ar- H_2 discharge, compared to the pure Ar discharge. However, as far as the loss is concerned, there are some extra important loss mechanisms in the Ar- H_2 discharge. Indeed, in the pure Ar discharge, the loss of electrons is almost exclusively caused by diffusion to the walls and subsequent recombination at the walls, because electron- Ar^+ -ion recombination in the plasma is not important (due to the low rate coefficient). In the Ar- H_2 discharge, on the other hand, electron-ion recombination with ArH^+ and H_3^+ ions plays an important role, because the rate coefficients for dissociative recombination with molecular ions are significantly higher. Hence, these additional loss mechanisms explain the drop in electron density.

Similarly, the drop in Ar^+ ion density as a function of H_2 addition is also caused by additional important loss mechanisms in the Ar- H_2 discharge, and by the absence of additional significant production mechanisms. Indeed, electron impact ionization of Ar atoms, and to a less extent, fast Ar^+

ion and Ar atom impact ionization, are again the dominant production mechanisms, both in the pure Ar discharge and in the Ar-H₂ mixture. The loss of Ar⁺ ions, on the other hand, is mainly attributed to diffusion and recombination at the walls in the pure Ar discharge, whereas in the Ar-H₂ discharge, charge transfer and especially H-atom transfer between Ar⁺ ions and H₂ molecules (giving rise to H₂⁺ and ArH⁺ ions, respectively) cause an additional loss of the Ar⁺ ion density.

A drop in these species densities was also experimentally observed in the literature [1–4], based on mass spectrometry or Langmuir probe measurements, but several different explanations were suggested, e.g., a drop in electron temperature and ion-molecule reactions [1], stepwise ionization into highly excited Ar states, followed by quenching down to the Ar (4s) metastable levels [4], or fast recombination via molecular ions [2,3]. The explanation given in Ref. [3], albeit for a different discharge plasma (i.e., a cascaded arc plasma), i.e., H-atom transfer between Ar⁺ and H₂ gives rise to loss of Ar⁺ ions and the formation of ArH⁺ ions, which can then recombine rapidly with electrons, is in agreement with our model observations. Hence, this shows the usefulness of our model to predict reaction rates in a quantitative manner, which may help one to provide better insight in experimental observations.

When comparing Figs. 3(a) and 3(b), it is clear that the drop in densities is more significant for the Ar⁺ ions than for the electrons. The reason is that the densities of the hydrogen-related ions, i.e., ArH⁺, H⁺, H₂⁺, and H₃⁺ (Figs. 3(c)–(f)) increase with H₂ addition, for obvious reasons. The effect is most pronounced for the H⁺, H₂⁺, and H₃⁺ ions, and is slightly less significant for the ArH⁺ ions. Indeed, the latter are created by H-atom transfer between Ar⁺ ions and H₂ molecules. Hence, when H₂ is added to the Ar discharge, on one hand, the H₂ concentration increases, but on the other hand, the Ar⁺ ion density decreases, so that the production increases less than an order of magnitude (as would be expected from the increase in H₂ concentration). As a result of the increase of the hydrogen-related ion densities with H₂ addition, and because the electron density should be equal to the total ion density in the bulk plasma, the electron density drops indeed more slowly than the Ar⁺ ion density.

Keeping in mind that the fluxes of the electrons and the various ions are proportional to the species densities, it is expected that the total electrical current (which is calculated from the sum of the fluxes of the charged species) decreases with rising H₂ addition. Indeed, the rise in fluxes of the hydrogen-related ions appears to be not significant enough to compensate for the drop in electron and Ar⁺ ion fluxes. The effect is, however, not so big, i.e., the electrical current was calculated to be 5.3 mA in the pure argon discharge for the conditions under study, and it drops to 5 mA at 0.1% H₂ addition and 4.7 mA at a H₂ concentration of 1%.

Figure 4 illustrates the calculated one-dimensional density profiles of the H atoms (a), Ar metastable atoms (b), sputtered Cu atoms (c), and Cu⁺ ions (d), for 0%, 0.1%, and 1% H₂ addition. As expected, the density of the H atoms [Fig. 4(a)] increases with H₂ addition. The increase is a factor of 6,

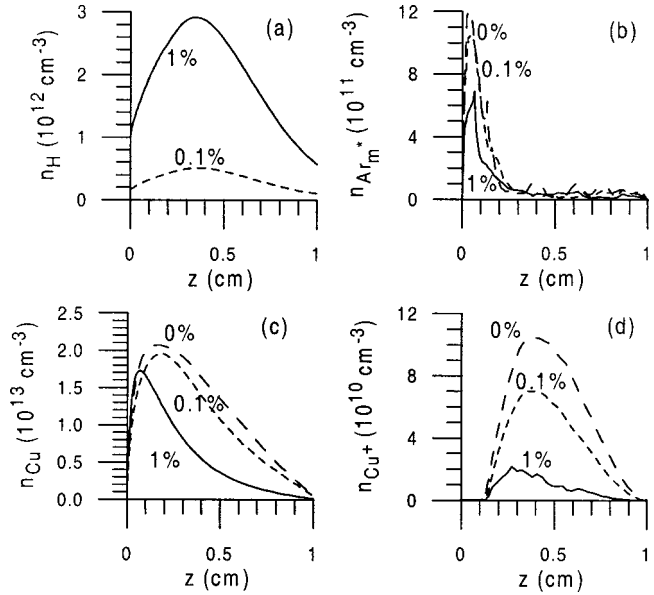
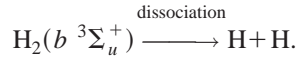
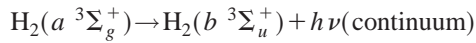
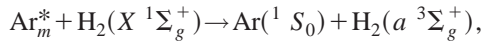


FIG. 4. Calculated one-dimensional density profiles (at the cell axis) of the H atoms (a), Ar metastable atoms (b), sputtered Cu atoms (c), and Cu⁺ ions (d), in an Ar glow discharge with 1% H₂ addition (solid lines) and 0.1% H₂ addition (small dashed lines), and in a pure Ar discharge (wide dashed lines) at 800 V, 1 Torr, and 300 K.

for an increase in H₂ addition of a factor of 10 (i.e., ca. $5 \times 10^{11} \text{ cm}^{-3}$ at 0.1% H₂, and ca. $3 \times 10^{12} \text{ cm}^{-3}$ at 1% H₂ addition), hence somewhat less than linearly. The calculated H₂ density, on the other hand, increases linearly with the percentage H₂. Indeed, in spite of the large number of production and loss processes taken into account in the H-H₂-fluid model (see Sec. II), the calculated H₂ density was found equal to the initial density given as input in the model, i.e., determined by the percentage H₂, multiplied with the gas density calculated from the ideal gas law (see above). This gives values of $3.2 \times 10^{13} \text{ cm}^{-3}$ at 0.1% and $3.2 \times 10^{14} \text{ cm}^{-3}$ at 1% H₂, found to be constant in space (and therefore not shown here). The H atom density increases, therefore, less rapidly than the H₂ density, or in other words, the dissociation degree drops slightly with H₂ addition (from about 0.6% at 0.1% H₂ addition, to about 0.35% at 1% H₂ addition). The reason is found in the dominant production of H atoms from dissociative excitation of H₂ molecules by Ar metastable atoms. Indeed, the latter species, and hence this production rate, are becoming less important at high H₂ concentrations (see below), explaining the drop in dissociation degree.

It is worth mentioning here that our calculations predict, indeed, that the production of H atoms by dissociative excitation of H₂ due to Ar metastable atoms, is more important than electron impact dissociative excitation. This is in agreement with experimental observations of a strong continuum emission in the spectral range 220–440 nm, in Ar-H₂ glow discharges [14–16]. This continuum is considered to be the result of the sequence [14–16,27]



An alternative reaction path would be the excitation into the triplet state by electron impact, followed also by dissociation (i.e., reaction no. 9 of Table I). However, in Ne-H₂ mixtures, where excitation of the H₂ molecules by Ne metastables is not possible, no significant continuum was observed under similar experimental conditions [16]. This suggests, indeed, that electron impact dissociative excitation is less important than dissociative excitation by Ar metastables, in agreement with our model predictions.

As mentioned above, the calculated Ar metastable atom density drops at increasing H₂ concentration, as is apparent from Fig. 4(b). This is explained by the quenching of Ar metastables due to H₂ molecules (i.e., dissociative excitation of H₂ molecules to form H atoms; see above). This process, which is of course absent in a pure Ar discharge, is indeed found to be an important loss mechanism of the Ar metastable atoms in the Ar-H₂ discharge, especially at high H₂ concentrations, i.e., we calculated a relative contribution of about 10% at 0.1% H₂, and somewhat above 50% at 1% H₂ addition.

Finally, the sputtered Cu atom and Cu⁺ ion density profiles are shown for 0%, 0.1%, and 1% H₂ addition in Figs. 4(c) and 4(d). It appears that the addition of H₂ also causes a drop in the densities of these species. The drop in the Cu atom density is attributed to the somewhat lower sputtering flux at rising H₂ concentrations. Indeed, the sputtering flux was calculated to be $5.4 \times 10^{16} \text{ s}^{-1}$ in the pure Ar discharge, and this value drops to $4.5 \times 10^{16} \text{ s}^{-1}$ at 0.1% H₂, and $3.9 \times 10^{16} \text{ s}^{-1}$ at 1% H₂ addition. The reason for this drop is the lower flux of Ar⁺ ions and fast Ar atoms bombarding the cathode at increasing H₂ concentrations. Indeed, both these species play the most significant role in sputtering, even at considerable H₂ additions. The relative contributions of fast Ar atoms and Ar⁺ ions are calculated to be about 78% and 17%, respectively (both decreasing a few percentages with the H₂ addition rising till 1%). The two other species playing a non-negligible role in sputtering, are the Cu⁺ ions (so-called self-sputtering, with a relative contribution calculated to be around 3–5%, again slightly decreasing with rising H₂ addition) and the ArH⁺ ions. The latter species, of course, do not come into play in the pure Ar discharge, but their relative contribution is calculated to be 1.2% at 0.1% H₂ addition, and it rises to 7.5% at 1% H₂ addition.

Hence, in spite of the lower ArH⁺ flux bombarding the cathode, the ArH⁺ ions play a significant role in the sputtering process in Ar-H₂ glow discharges, at considerable H₂ concentrations. The reason is that they are characterized by higher energy, and that the sputtering efficiency rises with energy of the bombarding species, in the energy range of interest here. This phenomenon of the higher kinetic energy of ArH⁺ ions compared to Ar⁺ ions when bombarding the

cathode, and hence the important role of ArH⁺ ions to sputtering in an Ar-H₂ discharge, has also been reported in the literature [6]. It was even found [6] that, because of this reason, for certain conditions the sputter rates can reach a maximum at 5–20% hydrogen added to the argon discharge.

As far as the other three hydrogen-related ions (H⁺, H₂⁺, and H₃⁺) are concerned, their contribution to sputtering is found to be of minor importance compared to the role of fast Ar⁰ atoms, Ar⁺, Cu⁺, and ArH⁺ ions at the conditions under study, i.e., with relative contributions calculated to be 0.03%, 0.02%, and 0.04% for H⁺, H₂⁺, and H₃⁺, respectively, at 1% H₂ addition. This is explained by their low fluxes when bombarding the cathode, in combination with their low sputtering efficiency (due to their low mass).

The Cu⁺ ion density also decreases with H₂ addition, and the drop is clearly more pronounced than for the Cu atoms. This is attributed to the decreased efficiency of ionization of the Cu atoms in the model. Indeed, both the Ar⁺ ion density and the Ar metastable density drop with adding H₂ to the discharge [see above, Figs. 3(b) and 4(b), respectively]. Hence, asymmetric charge transfer with Ar⁺ ions and Penning ionization by Ar metastable atoms, which are found to be the two most important ionization mechanisms of sputtered Cu atoms in a pure Ar glow discharge (see below), become less important with the addition of H₂. Electron impact ionization becomes also slightly less important, because of the somewhat lower electron flux, but the effect is less pronounced than for Penning ionization and asymmetric charge transfer. Hence, as far as the relative contributions of the three ionization mechanisms are concerned, it is found that Penning ionization and asymmetric charge transfer drop at rising H₂ addition, whereas electron impact ionization becomes relatively more important. Indeed, the relative contributions of asymmetric charge transfer, Penning ionization, and electron impact ionization were calculated to be 60%, 35%, and 5% in the pure Ar discharge, whereas at 1% H₂ addition, these values change to about 50%, 30%, and 20%, respectively, for the conditions under study.

This might explain some observations in the literature [17,18] that a better correlation could be obtained between measured relative sensitivity factors for different sputtered elements and values predicted by simple empirical equilibrium models, when adding H₂ to an argon glow discharge. Relative sensitivity factors are used for quantitative analysis in glow discharge mass spectrometry, and they are a measure for the ionization efficiency of the sputtered atoms in the plasma [79]. The above-mentioned equilibrium models [17,18] are based on the first ionization potential of the elements, which determines only the cross section of electron impact ionization. Indeed, Penning ionization occurs more or less unselectively (depending only on the mass and/or radius of the elements [80]), as long as the ionization potential of the elements is below the excitation energy of the Ar metastable atoms (i.e., 11.55 eV). This is the case for almost all elements, with the exception of nitrogen, oxygen, and chlorine [79]. Asymmetric charge transfer, on the other hand, is a very selective process, which depends on the availability of suitable energy levels of the element ions, which overlap

closely with the Ar^+ ion ground state (or metastable level) [79]. Hence, the better correlation with model predictions based on the first ionization potential in the Ar- H_2 glow discharge suggests that electron impact ionization plays a more important role as ionization mechanism of the sputtered atoms in the Ar- H_2 mixture, compared to a pure Ar discharge, which is in accordance with the trend that we have predicted by using our model (see above).

Besides the changing relative contributions of the three different ionization mechanisms of the Cu atoms, it remains true that the efficiency of the three ionization processes decreases in absolute values as a function of H_2 addition, and hence that the calculated ionization degree of Cu decreases. The ionization degree was calculated to be 0.4% in the pure Ar discharge, and this value drops to 0.3% at 0.1% H_2 concentration, and about 0.16% at 1% H_2 addition. Hence, it appears that the calculated ionization degree of Cu is only slightly lower but still in the same order of magnitude as the dissociation degree of H_2 (see above). The calculated ionization degree of argon, on the other hand, is still a few orders of magnitude lower (i.e., typically 10^{-5} at the conditions under study, see above), for the reasons given above.

IV. CONCLUSION

The effect of H_2 added to an Ar glow discharge is investigated by means of a hybrid modeling network. The latter consists of a number of MC and fluid models for the different species assumed to be present in the plasma, i.e., Ar gas atoms, electrons, Ar^+ ions, fast Ar atoms, ArH^+ , H^+ , H_2^+ and H_3^+ ions, H atoms and H_2 molecules, Ar metastable atoms, and sputtered Cu atoms and the corresponding Cu^+ ions. Sixty five different reactions between these species are taken into account, of which most are treated in the MC models. Typical calculation results of the model include the densities and fluxes of the various plasma species, the role of different production and loss processes for the various species, the cathode sputtering rate and contributions by different bombarding species, the dissociation degree of H_2 and the ionization degree of Ar and of sputtered Cu atoms.

As an illustration, the calculations are carried out for a mixture of Ar with 1% H_2 addition, and comparison is also made with a pure Ar discharge, and with 0.1% H_2 addition. It is found that the densities of electrons, Ar^+ ions, Ar metastable atoms, sputtered Cu atoms and corresponding Cu^+ ions all drop as a function of H_2 addition. A drop in electron and Ar^+ ion densities is also experimentally observed in the literature [1–4]. The reason for the drop in electron density is the electron recombination with ArH^+ and H_3^+ ions, whereas the drop in Ar^+ density is attributed to H-atom transfer of Ar^+ ions with H_2 molecules. The model predictions identify the reactions responsible for these effects, and these are in excellent agreement with experimental observation [3], albeit for different discharge conditions. The latter reaction mechanism between Ar^+ and H_2 leads to the formation of ArH^+ ions, which are therefore also characterized by a relatively high density in the Ar- H_2 discharge (i.e., calculated to be only a factor of 3 lower than the Ar^+ ion density,

at 1% H_2 addition). Also, the H_3^+ ions have a rather high density at 1% H_2 addition (i.e., comparable to the ArH^+ density), which is attributed to the efficient proton transfer reaction between ArH^+ and H_2 . The densities of H^+ and H_2^+ ions, on the other hand, are calculated to be several orders of magnitude lower. This calculation result of relatively high ArH^+ and H_3^+ ion densities and low H^+ and H_2^+ ion densities is also consistent with findings in the literature [7,37,38,74–77].

The calculated drop in Ar metastable atom density as a function of H_2 addition is due to collisions with H_2 molecules, leading to quenching of the Ar metastable level, as well as excitation followed by dissociation of H_2 . The latter is indeed found to be the most important mechanism for H_2 dissociation (and hence formation of H atoms), which is in excellent agreement with experimental observations in the literature of a strong continuum emission in the spectral range of 220–440 nm, typically observed in Ar- H_2 glow discharges [14–16]. The dissociation degree of H_2 was calculated around 0.35–0.6% at 1% and 0.1% H_2 addition, respectively. This suggests that at the conditions under study most of the added hydrogen is present in molecular form. Nevertheless, the H atom density is still quite significant, and higher than the electron density or any of the ionic species densities.

Because the Ar^+ ion and fast Ar atom fluxes bombarding the cathode decrease with H_2 addition, the amount of sputtering drops and hence also the sputtered Cu atom density. Indeed, the sputtering is mainly caused by fast Ar atoms and (to a less extent) by Ar^+ ions. It should, however, be mentioned that the Cu^+ ions also play a non-negligible role (order of a few percentages), and the contribution of ArH^+ ions becomes also significant at 1% H_2 addition. The latter is attributed to the higher energy of the ArH^+ ions bombarding the cathode, in spite of their lower flux, and it is in correspondence with observations in the literature [6].

Finally, the drop in Cu^+ ion density as a function of H_2 addition is due to a combination of (i) the drop in Cu atom density and (ii) a drop in ionization efficiency of the Cu atoms. Indeed, the latter results from the lower Ar^+ ion and Ar metastable atom densities, leading to a drop in ionization of Cu atoms by asymmetric charge transfer with Ar^+ ions and Penning ionization by Ar metastable atoms (i.e., the two most important ionization mechanisms of Cu atoms). Electron impact ionization of Cu atoms also decreases slightly with H_2 addition, but the effect is less pronounced than for the other two ionization mechanisms. Hence, this means that the relative contributions of asymmetric charge transfer and Penning ionization drop, whereas electron impact ionization becomes relatively more important. The latter can explain some observations in the literature, with respect to a better correlation between measured relative sensitivity factors and values predicted by simple equilibrium models [17,18].

The above model predictions illustrate that our model can explain most of the effects observed experimentally in Ar- H_2 glow discharges. Exact quantitative comparison with experimental data could not be made, because of the general cell geometry used here as an example to illustrate the model results. The only experimental observation made in the lit-

erature, which cannot yet be predicted with our present model, is the fact that some optical emission lines drop in intensity whereas other line intensities show a rise as a function of H₂ addition. Indeed, this can only be explained when comparing in detail the energy levels of H atoms and H₂ molecules, with the energy level schemes of the elements concerned, because a selective mechanism (population or quenching of certain energy levels) is expected to play a role. Such a study is planned for the near future, based on a systematic experimental survey.

ACKNOWLEDGMENTS

A.B. is indebted to the Flemish Fund for Scientific Research (FWO) for financial support. This research is also sponsored by the Federal Services for Scientific, Technical and Cultural affairs (DWTC/SSTC) of the Prime Minister's Office through IUAP-IV (Conv. P4/10). Finally, we are very thankful to A. V. Phelps, for supplying us with the necessary data, for reading the manuscript, and for the many interesting discussions.

-
- [1] P. F. Knewstubb and A. W. Tickner, *J. Chem. Phys.* **36**, 674 (1962).
- [2] M. H. Gordon and C. H. Kruger, *Phys. Fluids B* **5**, 1014 (1993).
- [3] R. F. G. Meulenbroeks, A. J. van Beek, A. J. G. van Helvoort, M. C. M. van de Sanden, and D. C. Schram, *Phys. Rev. E* **49**, 4397 (1994).
- [4] R. S. Mason, P. D. Miller, and I. P. Mortimer, *Phys. Rev. E* **55**, 7462 (1997).
- [5] F. L. Tabares and D. Tafalla, *J. Vac. Sci. Technol. A* **14**, 3087 (1996).
- [6] C. V. Budtz-Jorgensen, P. Kringhoj, and J. Bottiger, *Surf. Coat. Technol.* **116**, 938 (1999).
- [7] J. T. Gudmundsson, *Plasma Sources Sci. Technol.* **8**, 58 (1999).
- [8] A. Manenschijn, G. C. A. M. Janssen, E. van der Drift, and S. Radelaar, *J. Appl. Phys.* **69**, 1253 (1991).
- [9] S. B. Radovanov, J. K. Olthoff, R. J. Van Brunt, and S. Djurovic, *J. Appl. Phys.* **78**, 746 (1995).
- [10] M. Capitelli and M. Dilonardo, *Chem. Phys.* **24**, 417 (1977).
- [11] M. Kuraica and N. Konjevic, *Phys. Rev. A* **46**, 4429 (1992).
- [12] M. Kuraica, N. Konjevic, M. Platisa, and D. Pantelic, *Spectrochim. Acta, Part B* **47**, 1173 (1992).
- [13] R. Videnovic, N. Konjevic, and M. Kuraica, *Spectrochim. Acta, Part B* **51**, 1707 (1996).
- [14] V.-D. Hodoroaba, V. Hoffmann, E. B. M. Steers, and K. Wetzig, *J. Anal. At. Spectrom.* **15**, 951 (2000).
- [15] V.-D. Hodoroaba, V. Hoffmann, E. B. M. Steers, and K. Wetzig, *J. Anal. At. Spectrom.* **15**, 1075 (2000).
- [16] V.-D. Hodoroaba, E. B. M. Steers, V. Hoffmann, and K. Wetzig, *J. Anal. At. Spectrom.* **16**, 43 (2001).
- [17] R. W. Smithwick III, D. W. Lynch, and J. C. Franklin, *J. Am. Soc. Mass Spectrom.* **4**, 278 (1993).
- [18] M. Saito, *Anal. Chim. Acta* **355**, 129 (1997).
- [19] B. Müller, Ch. Ottinger, and M. Yang, *Z. Phys. A* **320**, 61 (1985).
- [20] M. A. A. Clyne, M. C. Heaven, K. D. Bayes, and P. B. Monkhouse, *Chem. Phys.* **47**, 179 (1980).
- [21] K. R. Ryan and I. G. Graham, *J. Chem. Phys.* **59**, 4260 (1973).
- [22] P. Tosi, *Chem. Rev.* **92**, 1667 (1992).
- [23] N. Sadeghi and D. W. Setser, *Chem. Phys.* **95**, 305 (1985).
- [24] N. G. Adams, D. K. Bohme, D. B. Dunkin, and F. C. Fehsenfeld, *J. Chem. Phys.* **52**, 1951 (1970).
- [25] A. E. Roche, M. M. Sutton, D. K. Bohme, and H. I. Schiff, *J. Chem. Phys.* **55**, 5480 (1971).
- [26] V. Aquilanti, A. Galli, A. Giardini-Guidoni, and G. G. Volpi, *J. Chem. Phys.* **43**, 1969 (1965).
- [27] C. R. Lishawa, J. W. Feldstein, T. N. Stewart, and E. E. Muschlitz, Jr., *J. Chem. Phys.* **83**, 133 (1985).
- [28] B. L. Peko, R. L. Champion, and Y. Wang, *J. Chem. Phys.* **104**, 6149 (1996).
- [29] B. L. Peko and R. L. Champion, *J. Chem. Phys.* **107**, 1156 (1997).
- [30] I. N. Brovikova, E. G. Galiaskarov, A. M. Islyaikin, and V. I. Svetsov, *High Temp.* **37**, 503 (1999).
- [31] A. Bogaerts and R. Gijbels, *J. Anal. At. Spectrom.* **15**, 441 (2000).
- [32] K. Hassouni, T. A. Grotjohn, and A. Gicquel, *J. Appl. Phys.* **86**, 134 (1999).
- [33] B. Gordiets, M. Pinheiro, E. Tatarova, F. M. Dias, C. M. Ferreira, and A. Ricard, *Plasma Sources Sci. Technol.* **9**, 295 (2000).
- [34] P. H. de Haan, G. C. A. M. Janssen, H. J. Hopman, and E. H. A. Granneman, *Phys. Fluids* **25**, 592 (1982).
- [35] C. F. Chan, C. F. Burrell, and W. S. Cooper, *J. Appl. Phys.* **54**, 6119 (1983).
- [36] O. Kukumasa, *J. Phys. D* **22**, 1668 (1989).
- [37] A. C. Dexter, T. Farrell, and M. I. Lees, *J. Phys. D* **22**, 413 (1989).
- [38] T. Simko, V. Martisovits, J. Bretagne, and G. Gousset, *Phys. Rev. E* **56**, 5908 (1997).
- [39] O. Leroy, P. Stratil, J. Perrin, J. Jolly, and Ph. Belenguer, *J. Phys. D* **28**, 500 (1995).
- [40] T. G. Beuthe and J.-S. Chang, *Jpn. J. Appl. Phys., Part 1* **38**, 4576 (1999).
- [41] A. V. Phelps and Z. Lj. Petrovic, *Plasma Sources Sci. Technol.* **8**, R21 (1999).
- [42] H. Winter, F. Aumayr, and G. Lakits, *Nucl. Instrum. Methods Phys. Res. B* **58**, 301 (1991).
- [43] A. V. Phelps (private communication), and ftp://jila.colorado.edu/collision_data
- [44] H. A. Hyman, *Phys. Rev. A* **20**, 855 (1979).
- [45] H. A. Hyman, *Phys. Rev. A* **18**, 441 (1978).
- [46] S. J. Buckman and A. V. Phelps, *J. Chem. Phys.* **82**, 4999 (1985).
- [47] H. Tawara, Y. Itikawa, H. Nishimura, and M. Yoshino, *J. Phys. Chem. Ref. Data* **19**, 617 (1990).
- [48] A. G. Engelhardt and A. V. Phelps, *Phys. Rev.* **131**, 2115 (1963).
- [49] R. K. Janev and J. J. Smith, *Atomic and Plasma-Material In-*

- teraction Data for Fusion* (IAEA, Vienna, 1993), Vol. 4.
- [50] L. Vriens, Phys. Lett. **8**, 260 (1964).
- [51] A. Bogaerts, R. Gijbels, and W. J. Goedheer, J. Appl. Phys. **78**, 2233 (1995).
- [52] A. V. Phelps, J. Appl. Phys. **76**, 747 (1994).
- [53] A. V. Phelps, J. Phys. Chem. Ref. Data **20**, 557 (1991).
- [54] A. V. Phelps, J. Phys. Chem. Ref. Data **21**, 883 (1992).
- [55] P. S. Krstic and D. R. Schultz, Phys. Rev. A **60**, 2118 (1999); also: <http://www-cfadc.phy.ornl.gov/elastic/elasticAr.html>
- [56] A. V. Phelps, J. Phys. Chem. Ref. Data **19**, 653 (1990).
- [57] T. Tabata and T. Shirai, At. Data Nucl. Data Tables **76**, 1 (2000).
- [58] Z. Donko, Phys. Rev. E **64**, 026401 (2001).
- [59] Z. Lj. Petrovic, B. M. Jelenkovic, and A. V. Phelps, Phys. Rev. Lett. **68**, 325 (1992).
- [60] J. O. Hirschfelder, C. F. Curtiss, and R. B. Bird, *Molecular Theory of Gases and Liquids* (Wiley, New York, 1964).
- [61] K. B. McAfee, Jr., D. Sipler and D. Edelson, Phys. Rev. **160**, 130 (1967).
- [62] E. E. Ferguson, At. Data Nucl. Data Tables **12**, 159 (1973).
- [63] D. L. Albritton, At. Data Nucl. Data Tables **22**, 1 (1978).
- [64] D. L. Scharfetter and H. K. Gummel, IEEE Trans. Electron Devices **16**, 64 (1969).
- [65] L. G. Piper, J. E. Velazco, and D. W. Setser, J. Chem. Phys. **59**, 3323 (1973).
- [66] M. Bourène and J. Le Calvé, J. Chem. Phys. **58**, 1452 (1973).
- [67] J. E. Velazco, J. H. Kolts, and D. W. Setser, J. Chem. Phys. **69**, 4357 (1978).
- [68] B. J. Wood and H. Wise, J. Chem. Phys. **29**, 1416 (1958).
- [69] B. J. Wood and H. Wise, J. Phys. Chem. **65**, 1976 (1961).
- [70] A. Bogaerts and R. Gijbels, Phys. Rev. A **52**, 3743 (1995).
- [71] A. Bogaerts, M. van Straaten, and R. Gijbels, J. Appl. Phys. **77**, 1868 (1995).
- [72] A. Bogaerts and R. Gijbels, J. Appl. Phys. **79**, 1279 (1996).
- [73] N. Matsunami, Y. Yamamura, Y. Itikawa, N. Itoh, Y. Kazumata, S. Miyagawa, K. Morita, R. Shimizu, and H. Tawara, At. Data Nucl. Data Tables **31**, 1 (1984).
- [74] B. M. Penetrante and E. E. Kunhardt, J. Appl. Phys. **59**, 3383 (1986).
- [75] O. Luhr, Phys. Rev. **44**, 459 (1933).
- [76] J. Bretagne, G. Gousset, and T. Simko, J. Phys. D **27**, 1966 (1994).
- [77] P. H. Ratliff and W. W. Harrison, Spectrochim. Acta, Part B **49**, 1747 (1994).
- [78] A. Bogaerts and R. Gijbels, Anal. Chem. **68**, 2676 (1996).
- [79] A. Bogaerts and R. Gijbels, J. Anal. At. Spectrom. **11**, 841 (1996).
- [80] L. A. Riseberg, W. F. Parks, and L. D. Scheerer, Phys. Rev. A **8**, 1962 (1973).